

# Survey of Control Methods for Hypersonic Vehicles

Research Project Report, Course #085851

Ofir Vaknin

Adviser: Moshe Idan

December 2022

## Abstract

In this project, the longitudinal control of an air-breathing hypersonic Vehicle (AHV) is studied. Several studies that address the control of this highly nonlinear coupled system are reviewed. A broadly used nonlinear model of the AHV's aerodynamics is presented and reconstructed. This model is then verified and validated in comparison to previously known results. The model is linearized about a found trim condition and the linearized model is used to synthesize linear feedback controllers for the pitch angle and velocity of the vehicle. These controllers are tested in simulation on the nonlinear and linear models in several conditions. The results from these simulations are examined and evaluated, and the limitations of our control method are examined. Based on these results, the objectives of future work is obtained.

## 1 Introduction

In recent years, hypersonic flight has gained significant attention due to its promising applications in the civil and military fields [1]. Control of these scramjet-powered air-breathing hypersonic Vehicles (AHVs) is a complex task due to the highly nonlinear nature of their dynamics and the inherent coupling between their aerodynamics and propulsion. Several attempts were made to address the longitudinal control of such systems, the dynamic and aerodynamic modeling of which is extremely challenging.

In this project, a review of several such attempts was carried out. A widely used model of the longitudinal dynamics and aerodynamics of an AHV is presented in this report and reconstructed in simulation. This model will be verified by comparing trim conditions with the literature. The model is then linearized about a trim condition and the linearization is verified against results in the literature. The linearized model is an unstable MIMO system. The system is then stabilized using controllers for the pitch angle ( $\theta$ ) and the velocity ( $V$ ). The pitch angle  $\theta$  is controlled by the elevator angular deflection ( $\delta_e$ ) using a proportional and rate feedback controller. The velocity  $V$  of the vehicle is controlled using the normalized fuel equivalence ratio ( $\Phi$ ) with a proportional feedback controller. These controllers are then evaluated in

simulations of the linearized and original nonlinear models. The simulation results of a wide range of cases are presented and analyzed. Finally, conclusions based on the simulation analysis are derived and future work is discussed.

## 1.1 Literature Review

In this project, several previous studies of AHV control were considered. In [2] the longitudinal control of an AHV cruising at Mach 15 at an altitude of 110,000 ft is studied. The main focus of this article is on the robustness of the control system in the face of parameter uncertainty. The motion of the aircraft was modeled by nonlinear dynamic equations containing 28 uncertain parameters. The controllers were developed using genetic algorithms. They are based on the linear quadratic control scheme and include proportional-integral compensation. These controllers are tested using Monte Carlo evaluations with the goal of minimizing a stochastic cost function. The cost function is comprised of a stability metric and 38 step response performance metrics. Each criterion is assigned a weight which is chosen by the designer according to his demands. This control design scheme is evaluated in one flight condition, but, according to the writers, it can be applied to other flight conditions and then extended using gain scheduling.

The study in [3] uses a multi-input/multi-output adaptive sliding mode controller to control the longitudinal dynamics of an AHV. This is done in four main steps. First, the dynamics are linearized with respect to the velocity and altitude using full-state feedback. Then, a pure sliding mode controller is designed followed by the design of an adaptive sliding mode controller to improve the performance in the face of uncertainties. Finally, a sliding mode observer is designed to estimate the angle of attack and the flight path angle which are difficult to measure. The adaptive sliding mode controller was implemented with thin boundary layers around the sliding surfaces in order to avoid chattering of the controls. The controller is evaluated in a simulation involving model uncertainties and measurement noise in two scenarios: a 2000 feet altitude step and a 100 ft/sec velocity step response. The simulations show good tracking of these relatively low amplitude control inputs.

A complex high-fidelity nonlinear model of the AHV longitudinal dynamics was introduced in [4]. This model accounts also for the flexible structural modes of the vehicle. It is referred to as the Truth Model (TM) and is too complicated for control design. To simplify it, first, the aerodynamics and propulsion modules of the TM are approximated using a curve fit, rendering a reduced complexity model referred to as the Curve Fitted Model (CFM). The CFM is still too challenging for commonly used control design methods, partially due to its non-minimum phase characteristics. By removing the flexible states, assuming constant altitude (since it changes relatively slowly in comparison to other states), and neglecting the lift and drag forces generated by the elevator, a Control Oriented Model (COM) is derived. This model is suitable for control design using the standard feedback-linearization technique [5]. The performance and limitations of this controller were demonstrated within the TM simulation.

Numerous later studies proposed different control methods using the COM and CFM in the control design stage of their work. In [6] a canard was added to the

standard configuration of the AHV to counter the non-minimum phase characteristics of the system. The system was divided into the velocity, altitude and flight-path angle, and angle of attack and pitch rate subsystems. The CFM was used to synthesize a robust adaptive inversion controller for each subsystem. In [7] a controller for the velocity subsystem similar to the one used in [6] was suggested. Integral augmentation is implemented on the rest of the dynamics and the resulting systems are then controlled by adaptive controllers. The controllers from both articles were then evaluated in simulation on the TM. The maneuvers tested were similar involving simultaneous acceleration/deceleration and change of altitude. Both articles show good and comparable tracking performance of the desired altitude and velocity profiles.

## 1.2 Project Goals

This project has several main objectives. The first is to study the model used for the AHV dynamics. This is done by replicating the model using MATLAB/SIMULINK and validating it against previously attained results. Another objective is to study the different control methods used in the literature. This is done by reviewing the main studies published in the field and the methods they used. Finally, the main objective of this work is to examine the power of linear control in dealing with such a nonlinear problem. A linear control method is implemented, evaluated, and its limitations are examined. Based on these results, goals for the next steps of the research are defined.

## 2 The Model

In this section, we present the governing nonlinear equations of motion of the AHV. The reasons for using this model and the assumptions made are also explained. This model is used in the subsequent sections to find the trim conditions and for control design. This model was implemented using MATLAB/SIMULINK and is validated in the next section.

The model chosen in this study is the longitudinal control-oriented model (COM) presented in [4] with a few changes. The governing equations of the model are

$$\dot{V} = f_1 = \frac{1}{m} (T \cos(\alpha) - D) - g \sin(\theta - \alpha), \quad (1a)$$

$$\dot{\alpha} = f_2 = \frac{1}{mV} (-T \sin(\alpha) - L) + Q + \frac{g}{V} \cos(\theta - \alpha), \quad (1b)$$

$$\dot{Q} = f_3 = \frac{M}{I_{yy}}, \quad (1c)$$

$$\dot{\theta} = f_4 = Q, \quad (1d)$$

where

$$L = \frac{1}{2}\rho V^2 S C_L(\alpha, \delta_e), \quad (2a)$$

$$D = \frac{1}{2}\rho V^2 S C_D(\alpha, \delta_e), \quad (2b)$$

$$M = Z_T T + \frac{1}{2}\rho V^2 S \bar{c} [C_{M,\alpha}(\alpha) + C_{M,\delta_e}(\delta_e)], \quad (2c)$$

$$T = C_T^{\alpha^3} \alpha^3 + C_T^{\alpha^2} \alpha^2 + C_T^\alpha \alpha + C_T^0, \quad (2d)$$

and

$$C_L = C_L^\alpha \alpha + C_L^{\delta_e} \delta_e + C_L^0, \quad (3a)$$

$$C_D = C_D^{\alpha^2} \alpha^2 + C_D^\alpha \alpha + C_D^{\delta_e^2} \delta_e^2 + C_D^{\delta_e} \delta_e + C_D^0, \quad (3b)$$

$$C_{M,\alpha} = C_{M,\alpha}^{\alpha^2} \alpha^2 + C_{M,\alpha}^\alpha \alpha + C_{M,\alpha}^0, \quad (3c)$$

$$C_{M,\delta_e} = c_e \delta_e, \quad (3d)$$

$$C_T^{\alpha^3} = \beta_1 \Phi + \beta_2, \quad (3e)$$

$$C_T^{\alpha^2} = \beta_3 \Phi + \beta_4, \quad (3f)$$

$$C_T^\alpha = \beta_5 \Phi + \beta_6, \quad (3g)$$

$$C_T^0 = \beta_7 \Phi + \beta_8. \quad (3h)$$

$$(3i)$$

All the constants in (1) to (3) can be found in the appendix.

The model above is the COM from [4] with the addition of the lift and drag forces generated by the elevator and so is of higher fidelity. This model was chosen for several reasons, the first being that the article only presents the trim of the TM. As said before, the TM also includes states of the structural dynamics of the AHV. Since those states are zero in trim conditions, the trim found in the next section is comparable to the one found in the article. Another reason for choosing this model is that in the mentioned article a feedback linearization controller is proposed and so a model with a full relative degree should be used. The linear control design adopted in the current study does not impose such a constraint on the model so we can use this higher-fidelity model.

We will use  $x = [V, \alpha, Q, \theta]^T$  as our state variables and  $u = [\Phi, \delta_e]^T$  as the inputs. In addition, full-state feedback is assumed.

### 3 The Trim Condition

In this section, a trim condition for the model is found. Using this trim we make sure that our model was implemented correctly by comparing its results to those published in [4]. The trim found is used to linearize the model in the next section.

The trim we are looking for is an equilibrium point of the system. An equilibrium point is considered a point in the state space of the system at which the derivatives in (1) are zero. For a system such as ours, there is an infinite number of such equilibrium points that represent straight and level flight in different conditions.

The trim condition is the one mentioned in [4] and summarized in Table 1. In the following sub-section, we show that our model yields a similar trim condition and comment on the differences.

Table 1: Trim Condition From [4].

State/input	Value
V	7702.0808 ft/sec
$\alpha$	1.5153 deg
$\theta$	1.5153 deg
Q	0 deg/sec
$\delta_e$	11.4635 deg
$\Phi$	0.2514

### 3.1 Finding and Validating the Trim

To find the trim of our implemented model, a cost function, defined by

$$J = \dot{x}^T A_w \dot{x} \quad (4)$$

is used. Here  $\dot{x}$  represents the time derivatives of the state space vector and  $A_w$  is a weight matrix. It is used to balance the difference in orders of magnitude between characteristic values of the different states. In the current study, it was chosen as  $A_w = \text{diag}(1, 1e4, 1e4, 1e4)$ . Our goal is to find the state that minimizes (4). If a true trim is found, this minimum is zero.

To find the trim condition of the states and outputs, we set  $V$ ,  $\alpha$ , and  $Q$  according to their values in Table 1 and find the remaining states and control inputs, i.e.,  $\theta$ ,  $\delta_e$ , and  $\Phi$ , using the MATLAB function `fminsearch`. The results are presented in Table 2.

Table 2: Trim Conditions From Our Model.

Set State	Value	Trimmed Variables	Value	Error %
V	7702.0808 ft/sec	$\theta$	1.6232 deg	7.34
$\alpha$	1.5153 deg	$\delta_e$	12.4895 deg	8.95
Q	0 deg/sec	$\Phi$	0.2665	6.00

In Table 2, we see that the trim condition found does not match exactly the trim condition in [4], but, it does resemble it pretty well. The difference between the two conditions can arise due to the use of different weight matrices. The article does not specify how exactly the trim was obtained and so we can not be sure. Another source of error can be that all the coefficients we used were given to a certain degree of accuracy.

According to [4] and the linearization in the next section, the system is unstable, and so is our trim. To check this statement, a simulation of the open loop system is conducted. The initial conditions and inputs are according to the trim in Table 2 with  $\alpha = \theta_{trim}$  ( $\theta_{trim}$  is  $\theta$  from Table 2). Figure 1 shows that over 5 seconds, the

state variables barely change from their nominal values, and further simulations show that for longer time spans they will diverge. This result validates our trim condition to be true since this is exactly the behavior we expected from an unstable equilibrium point.

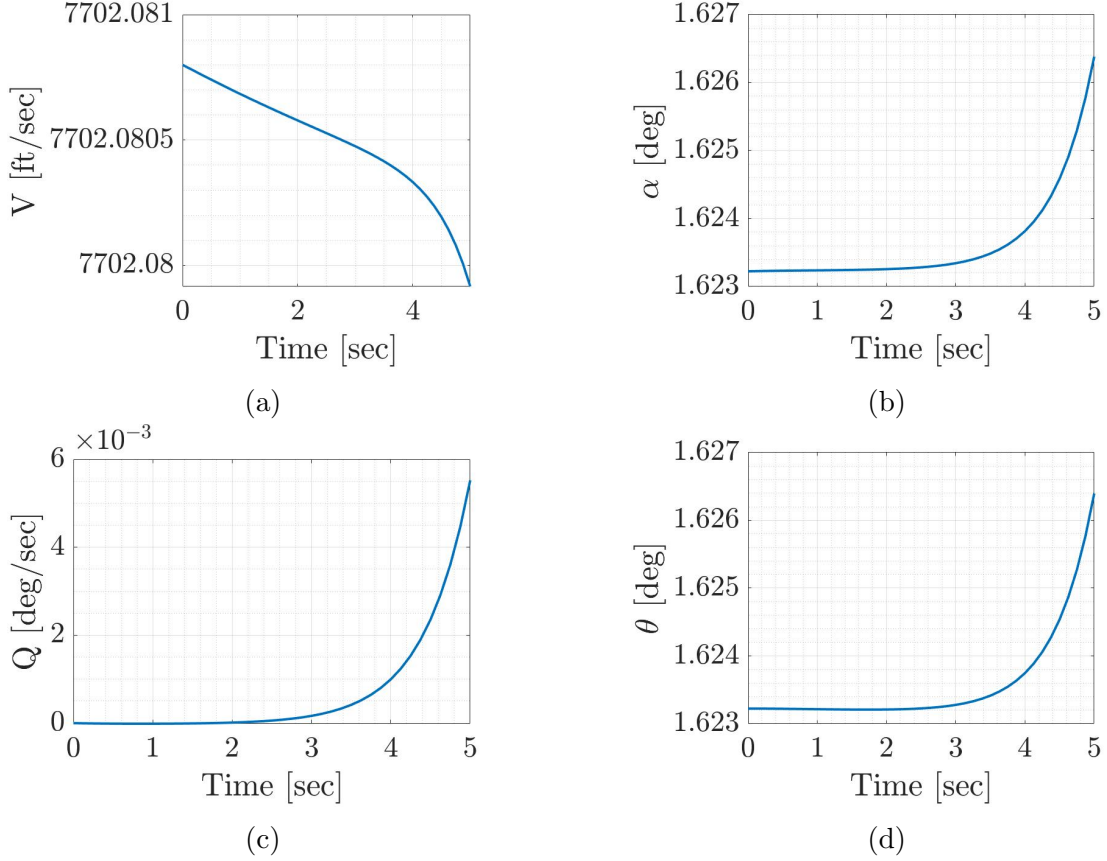


Figure 1: Open loop simulation at trim condition.

## 4 Linearization

In this section, the model from section 2 is linearized about the trim condition found in section 3. The linearized model obtained is validated in comparison to [4] and by analyzing the different elements of the matrices  $A$  and  $B$  derived. It is also used in the following sections to design and test the linear controllers.

The linearization was done numerically using MATLAB in the following manner. Let us denote  $x_t$  and  $u_t$  as the state variables and inputs of our model at the trim condition shown at Table 2. The linearized system matrices  $A$  and  $B$  are obtained numerically as

$$A_{ij} = \frac{f_i(x_t + e_j \cdot \delta_x, u_t) - f_i(x_t, u_t)}{\delta_x}, \quad \text{for } 1 \leq i \leq 4, 1 \leq j \leq 4, \quad (5)$$

and

$$B_{ij} = \frac{f_i(x_t, u_t + e_j \cdot \delta_u) - f_i(x_t, u_t)}{\delta_u}, \quad \text{for } 1 \leq i \leq 4, 1 \leq j \leq 2, \quad (6)$$

where  $f_i$ ,  $1 \leq i \leq 4$  are defined in (1),  $\delta_x = \delta_u = 1 \cdot 10^{-10}$  and  $e_j$  is the  $j$ -th unit vector. Note that smaller  $\delta_x, \delta_u$  were considered but did not yield different results. The numerical linearization resulted in the matrices

$$A = \begin{bmatrix} -0.0015 & 19.95 & 0 & -31.90 \\ -1.06 \cdot 10^{-6} & -0.0697 & 1.00 & 0 \\ -7.71 \cdot 10^{-6} & 2.981 & 0 & 0 \\ 0 & 0 & 1 & 0 \end{bmatrix} \quad (7)$$

and

$$B = \begin{bmatrix} 24.65 & -40.54 \\ -9.07 \cdot 10^{-5} & -0.0112 \\ 0.1237 & -1.491 \\ 0 & 0 \end{bmatrix}. \quad (8)$$

The matrices we got are reasonable and we indeed got the relations we were looking for between  $Q$ ,  $\dot{\theta}$ , and  $\dot{\alpha}$ . Another safety check is that the signs of the dependency of  $\dot{V}$  on  $\alpha$  and  $\theta$  are opposite.

To further validate our linearization, we compare our pole/transmission zero map (Fig. 2) to Fig. 3 which was found in [4]. To do so we matched the output used in the article, and so for this assessment  $y = [V, \gamma]$ . Examining both maps, we find that there are four more zeros and poles in Fig. 3. These zeros and poles arise from the flexible modes which are taken into account in the CFM and are neglected in our model. Apart from this difference, the two maps look to match fairly well. Although We were not able to find documentation of the exact coordinates of the poles and zeros in Fig. 3, we can clearly see that the zeros and poles look to be at similar locations.

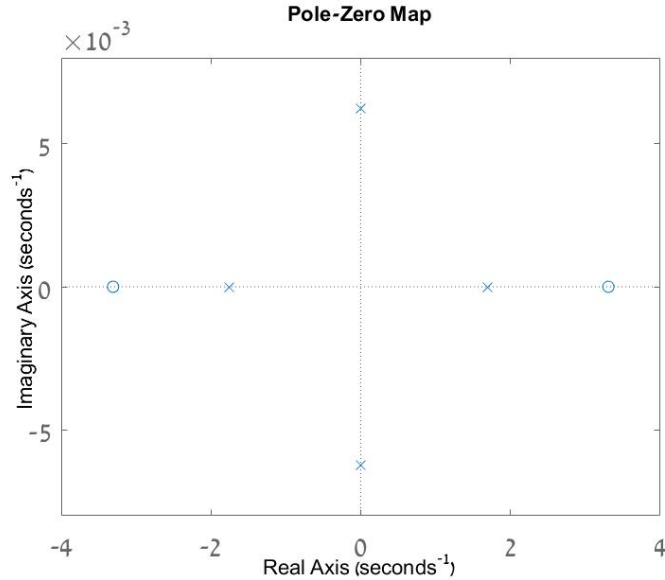


Figure 2: Pole/transmission zero map of our linearized model.

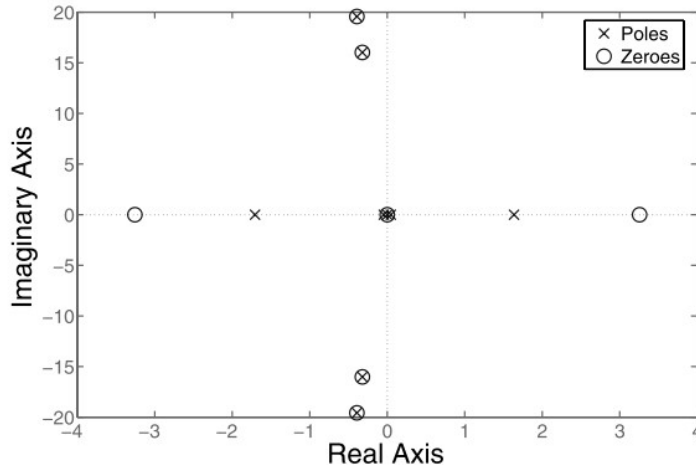


Figure 3: Pole/transmission zero map of the Jacobian linearization of the CFM, taken from [4].

The pole/transmission zero map in Fig. 2 shows that our linear model is non-minimum phase and unstable. In particular, the phugoid is very lightly damped while the short period is unstable. These results are consistent with the simulation in section 3 and with [2-4, 6, 7] making the system difficult to control. We deal with these problems in the following section by using specific transfer functions to control our system.

## 5 Controller Design

In this section, two controllers are designed to stabilize the unstable linear model obtained in section 4. Our system, as mentioned before, has two inputs  $\Phi$  and  $\delta_e$  and our goal is to control two states  $V$  and  $\theta$ . As one would expect, the first controller uses  $\Phi$  as input to control  $V$ . This is achieved by using a proportional controller. The second uses  $\delta_e$  to control  $\theta$ . This is done by using a proportional controller with rate feedback on the states  $\theta$  and  $Q$ . These controllers are simulated in the following section in different scenarios on the nonlinear model mentioned in section 2 and on the linear model obtained in section 4.

### 5.1 Controlling the Velocity

In this sub-section, the controller for  $V$  is designed using the input  $\Phi$ . The goal of this controller is to improve the damping of the phugoid mode of the system. By looking at the Root-Locus used to design the proportional controller, depicted in Fig. 4, it is apparent that this controller can not stabilize our plant. This is because of the proximity between the unstable pole and zero in the right half plane. One can suggest using more elaborate control methods such as adding lead/lag compensators. However, this approach will not resolve this stability issue, and will only make the control design more complex. The latter will be addressed by the subsequent pitch-angle controller, and hence is not considered critical at this stage of the multi-loop

controller design. As stated earlier, the goal of this controller is only to improve the characteristics of the phugoid ensuring better tracking of  $V$ . This can be easily achieved by the proportional controller that moves the two complex poles further to the left, as is shown in Fig. 5.

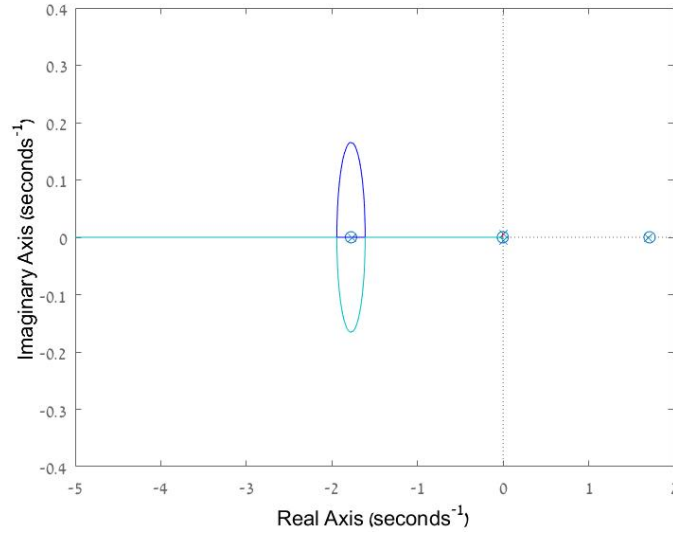


Figure 4: Root locus used to design the proportional controller for  $V$ .

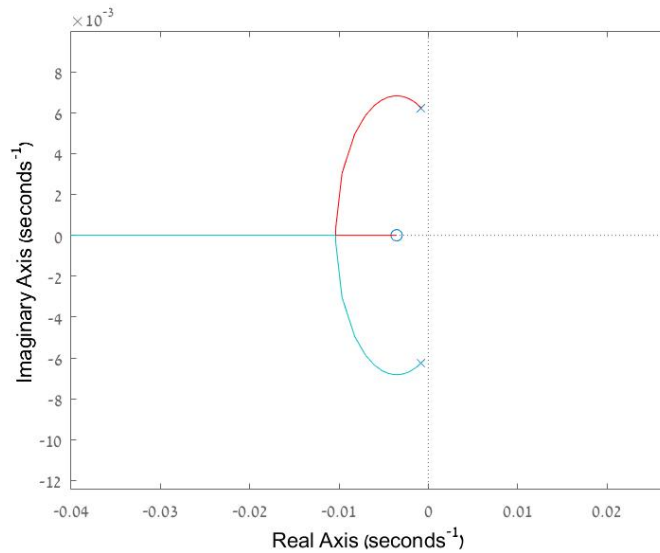


Figure 5: Closeup of Fig. 4.

By using the control law  $\Phi = K_v(V_{com} - V)$  with  $K_v = 7.622 \cdot 10^{-4}$  we move the poles from  $-8.5 \cdot 10^{-4} \pm 6.26 \cdot 10^{-3}j$ , i.e., damping of  $\zeta = 0.135$ , to both being on the real axis at  $-0.0104$ . This means we were able to make these poles about two times faster which helps us in the design of the pitch angle controller. For the latter, we

close the velocity control loop to yield

$$\dot{x} = (A - K_v B_1 C_v) x + K_v B_1 V_{com} + B_2 \delta_e, \quad (9)$$

where  $A$  is given in (7),  $B_1$  and  $B_2$  are the first and second columns of  $B$  found in (8),  $C_v = [1, 0, 0, 0]$ , and  $V_{com}$  is the velocity command. This is the model used to design the following control loop.

## 5.2 Controlling the Pitch Angle

In this sub-section, the controller for  $\theta$  is designed using the input  $\delta_e$ . A first attempt would be to design a proportional controller. The associated Root locus, depicted in Fig. 6, demonstrates why this approach would not work. Although the non-minimum phase zero is canceled due to the dynamics, the system is still unstabilizable for any gain.

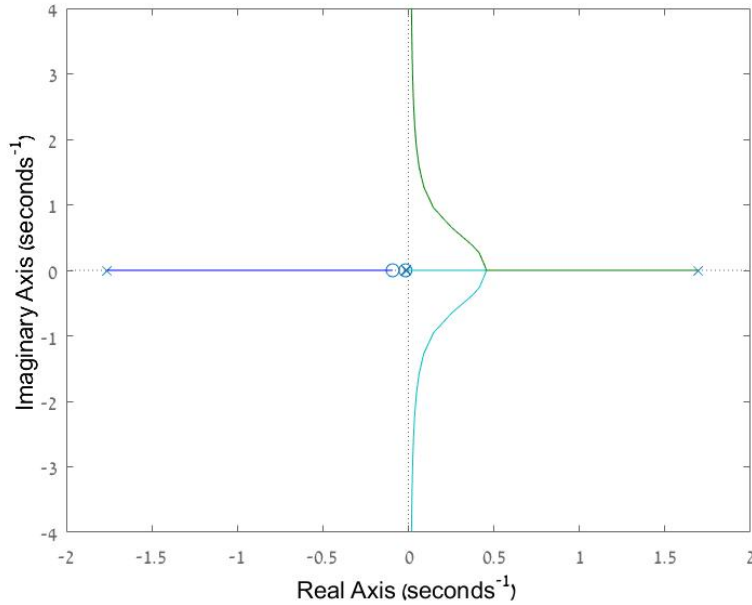


Figure 6: Zero angle root locus of a proportional controller for  $\theta$ .

To solve this issue and stabilize the system, we use a proportional controller with a rate feedback on the pitch rate  $Q$ , as depicted in Fig. 7. The controller gains were chosen by an iterative process after combining the two loops and using the Root Locus plot similar to the one presented in Fig. 8. In that figure, the location of the zero depicted in red is determined by the ratios between the two gains. After several iterations, we chose the control law  $\delta_e = K_Q (K_\theta (\theta_{com} - \theta) - Q)$  where  $K_Q = -10.246$  and  $K_\theta = 0.7842$ . Clearly, the resulting closed-loop system is stable.

The two controllers synthesized in this section are implemented and simulated using MATLAB/SIMULINK in the next section.

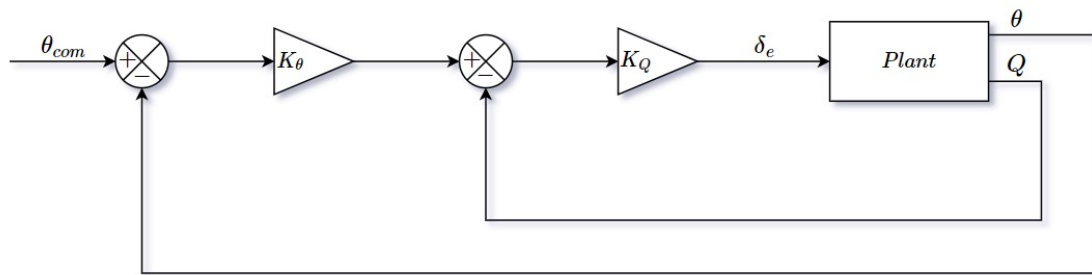


Figure 7: Schematic block diagram of the pitch angle controller.

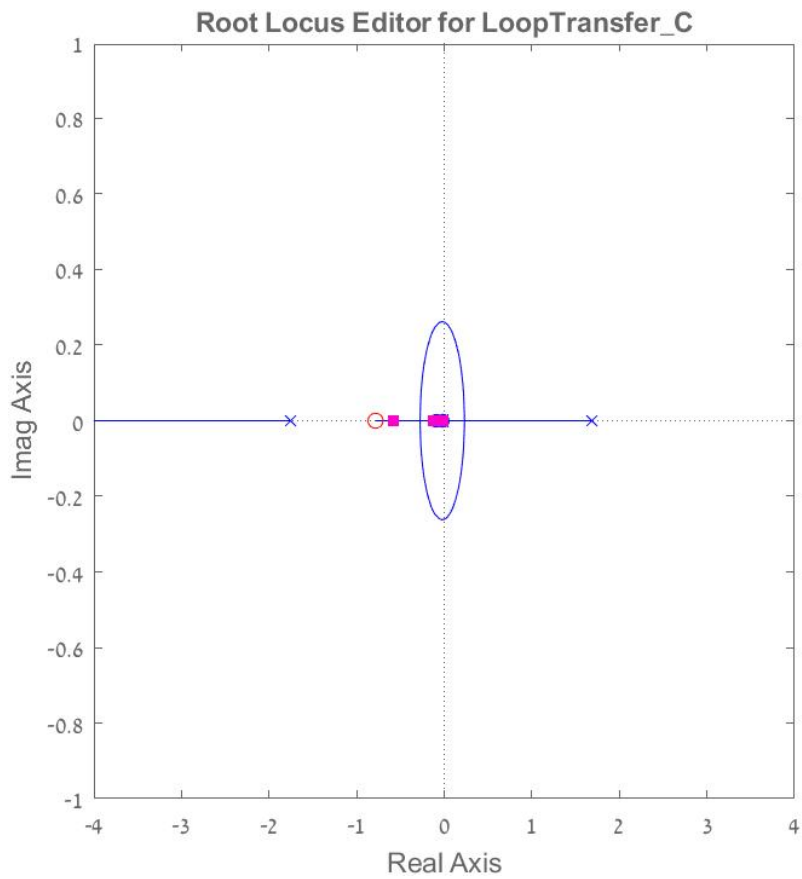


Figure 8: Zero angle root locus of the proportional-rate-feedback controller for  $\theta$ .

## 6 Results and Simulations

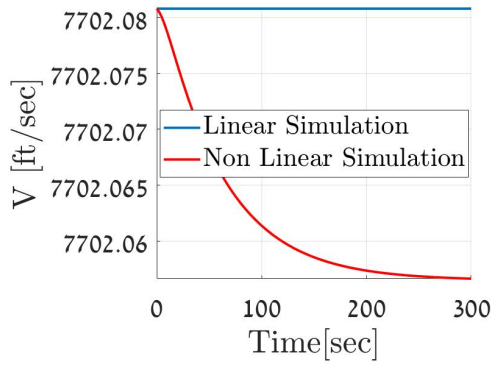
In this section, the controllers designed in section 5 are tested in simulation on the nonlinear presented in section 2 and on the linear model obtained in section 4. The results of these simulations are analyzed and explained. All simulations involve using first-order transfer functions with a pole at  $-2$  and unity DC-Gain as pre-filters to smooth the input command signals. The simulations also assume ideal servos and no time delays. The allowed deflection angle of the elevator is  $\delta_e \leq |20^\circ|$  and  $0 < \Phi < 1$ . Note that every command is referred to the system's trim state and is given at  $t = 1$  sec.

In Fig. 9 the initial conditions of the models are the trim conditions and there are no commands. The goal is to check if we were able to stabilize the system and to figure out whether the trim conditions of the linear and nonlinear models are the same. We see that the controlled system is stable and that both the linear and nonlinear models have very similar trim conditions. The differences result from the small non-zero optimization error when solving for the trim condition in section 3. These results also demonstrated that the linearization conducted in section 4 is sufficient to design a stabilizing controller of the system.

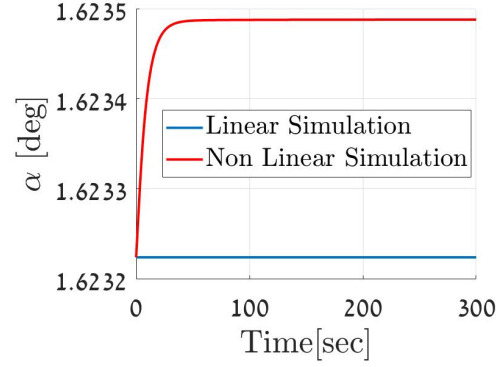
The next simulation also involves no input commands but the initial conditions are different from the trim values and are set according to the data in Table 3. Figure 10 demonstrates that even when the initial conditions are not at trim, the states and inputs converge to the trim values. This further validates the trim, linearization, and controller designs.

Table 3: Initial Conditions for Simulation Presented in Fig. 10.

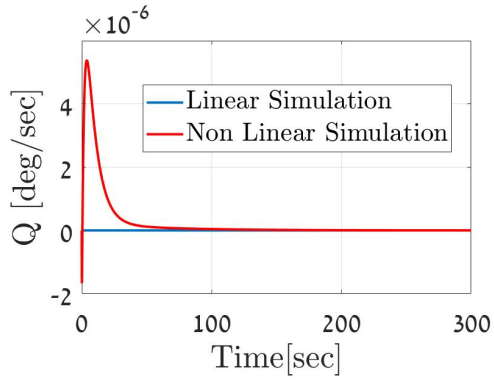
State	Initial Condition
V	7902.0808 ft/sec
$\alpha$	3.2464 deg
Q	1 deg/sec
$\theta$	4.8697 deg



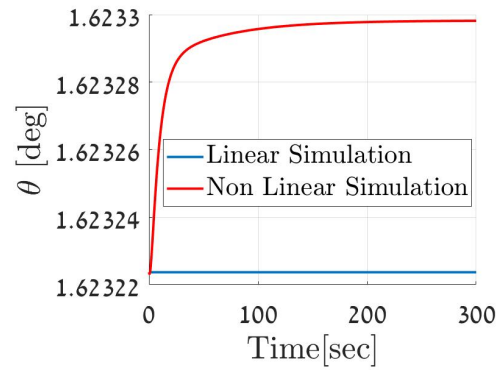
(a)



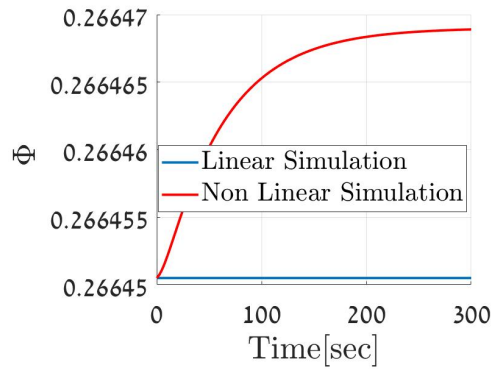
(b)



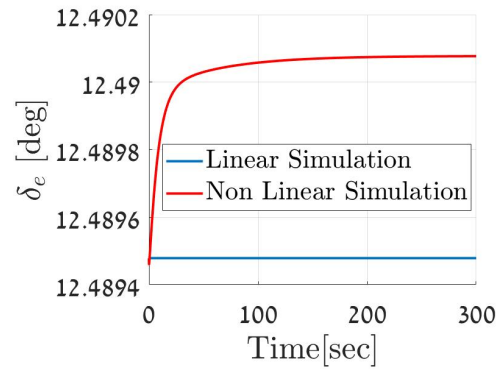
(c)



(d)

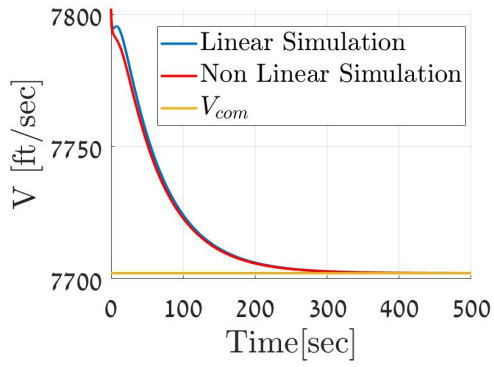


(e)

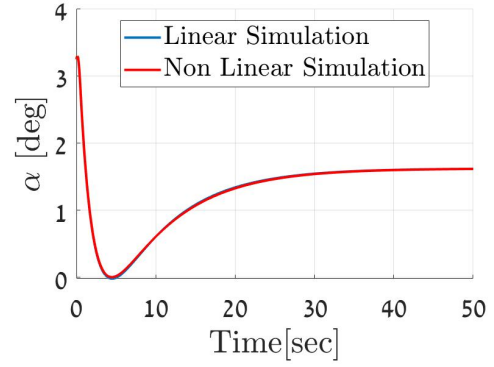


(f)

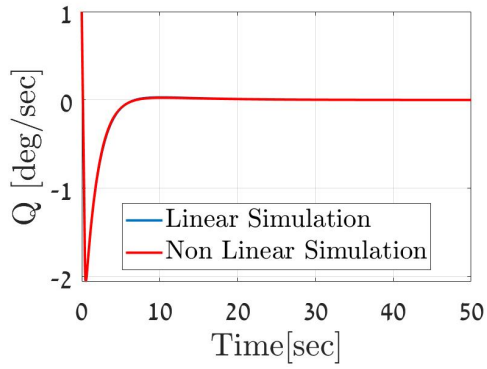
Figure 9: Response of States and Inputs to Trim Input Conditions.



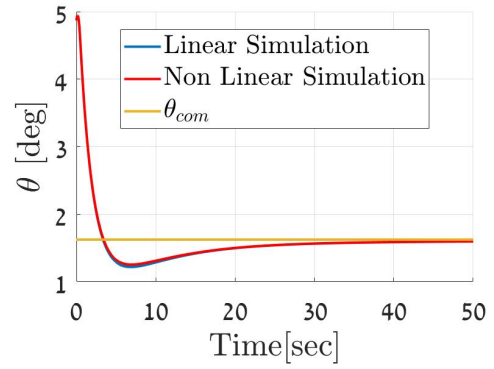
(a)



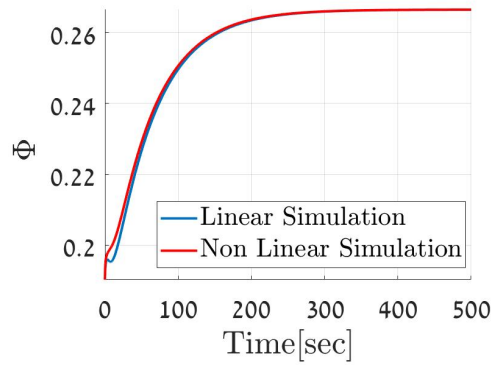
(b)



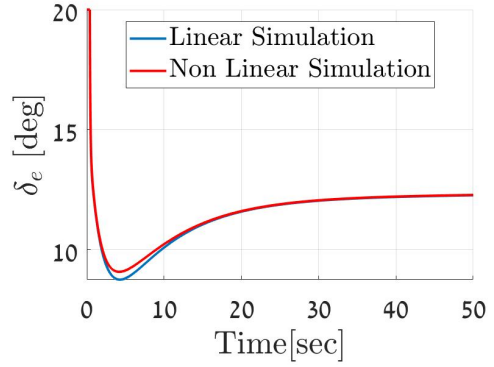
(c)



(d)



(e)



(f)

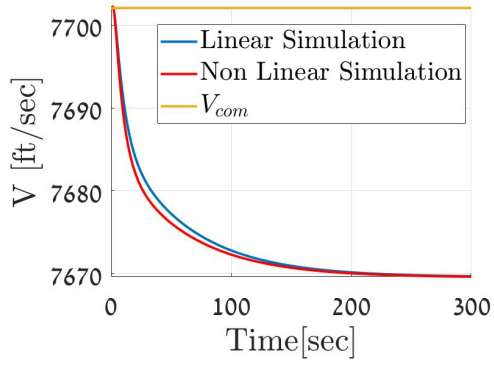
Figure 10: Response of States and Inputs to Non-Trim Initial Conditions.

Figures 11 to 13 show the systems  $1^\circ$ ,  $3^\circ$ , and  $5^\circ$   $\theta$  step responses with the initial conditions being the trim conditions. By examining Figs. 11d and 12d, it is apparent that the responses of the linear and nonlinear models are pretty similar although not the same. This behavior is expected since the linearization is more valid the closer we are to the trim conditions. Indeed, as  $V$  and  $\theta$  differ from the trim in (Figs. 12a and 12d) the responses of the linear and nonlinear models differ too. We also notice that the response of  $\theta$  is faster than that of  $V$  in all test cases examined. This matches the closed-loop pole locations of the designs presented in section 5.

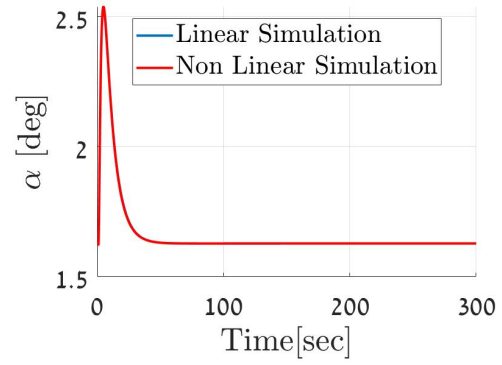
Another important result is the presence of steady-state errors as can be seen in Figs. 11a, 11d, 12a and 12d. This result is explained by the fact that neither of the controllers in section 5 uses integration control, the system doesn't have open-loop poles at the origin, and therefore the closed-loop system of type zero. The steady-state errors of  $\theta$  are negligible while those of  $V$  seem to get larger with the magnitude of the step input, with the error in Fig. 12a being 13%. Although those errors could be at least partially addressed with an integral controller, this was not performed in the current study, the aim of which was to demonstrate the limitations linear control methods when applied to the complicated nonlinear system addressed.

In Fig. 13 we see that the system diverges both for the linear and nonlinear models. This is expected and is due to the controllers being designed based on the linear model. This means that for too big a difference from the trim condition or too swift a maneuver, they are not able to stabilize the system. From Fig. 13f it is apparent that the input is saturated and the system is behaving as an open loop system. Note that the time scale in this figure is significantly smaller than in the others discussed and so the divergence is quick.

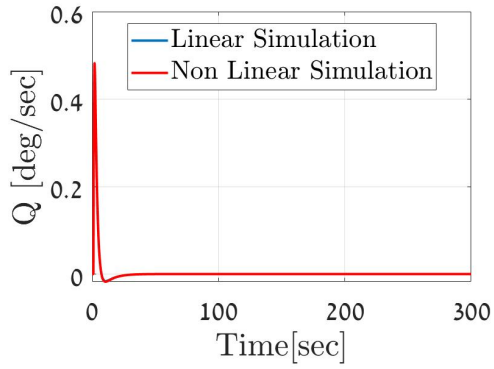
The conclusions arising from the above-shown results and from the previous sections are presented in the following section.



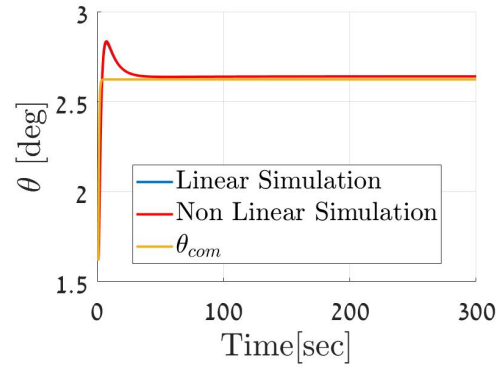
(a)



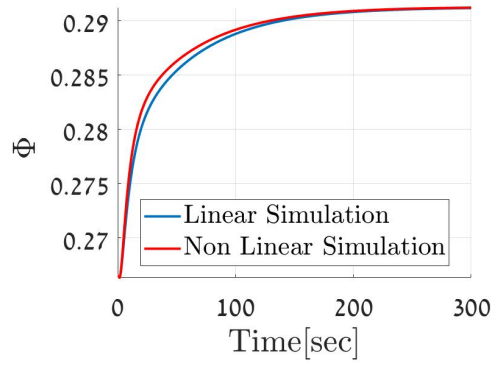
(b)



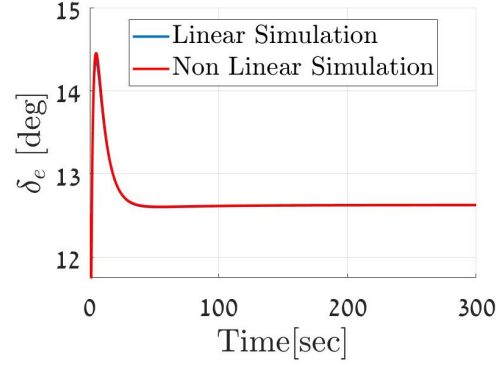
(c)



(d)

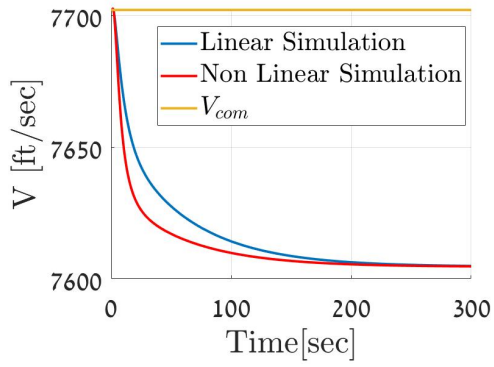


(e)

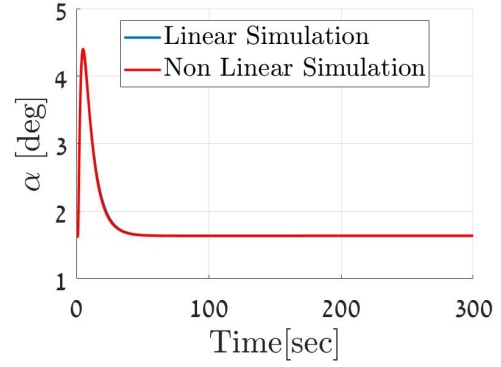


(f)

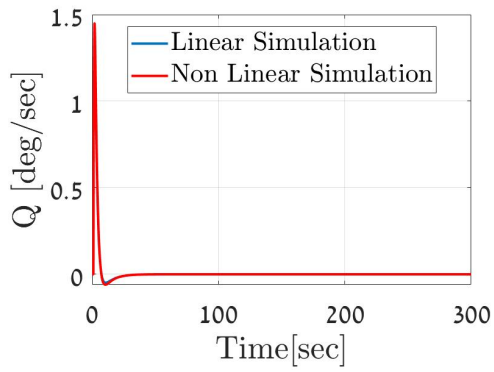
Figure 11: Response of States and Inputs to  $1^\circ \theta$  Step Command.



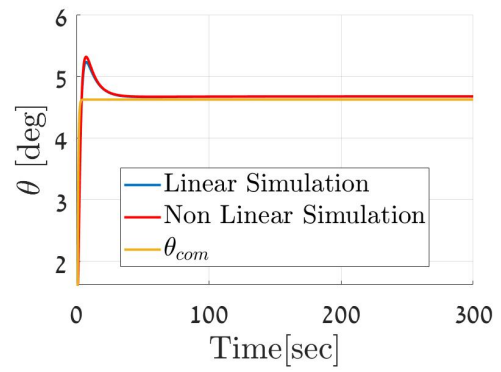
(a)



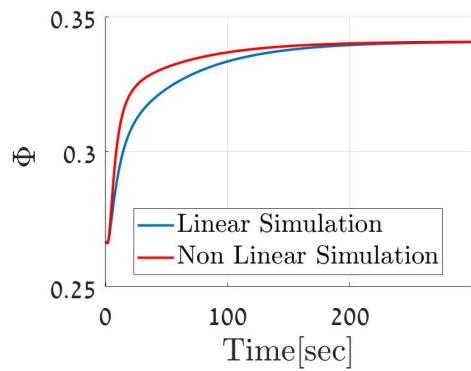
(b)



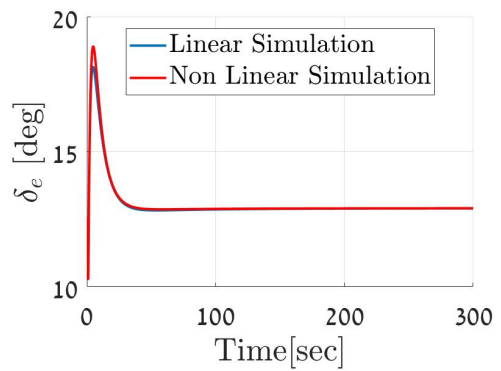
(c)



(d)

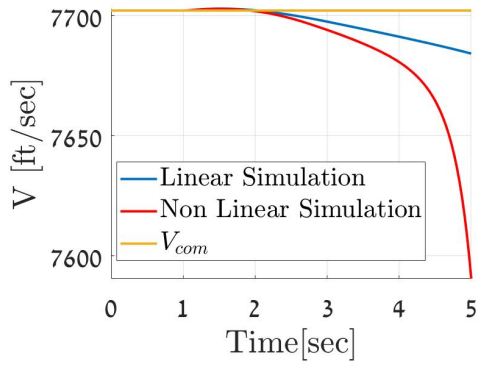


(e)

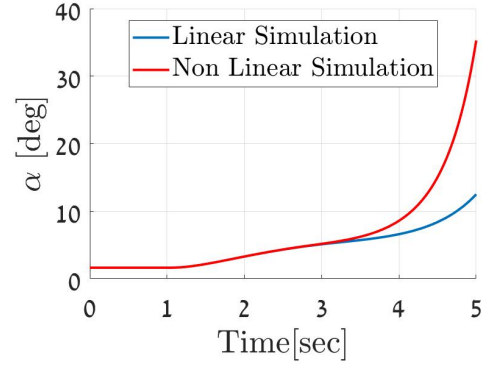


(f)

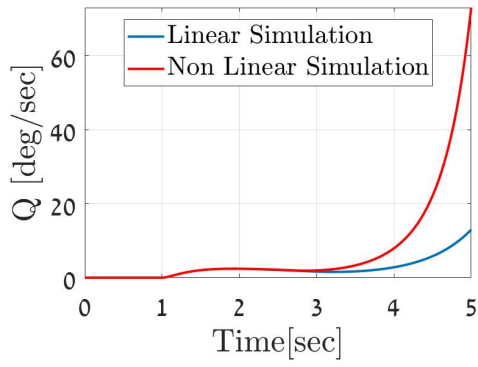
Figure 12: Response of States and Inputs to  $3^\circ \theta$  Step Command.



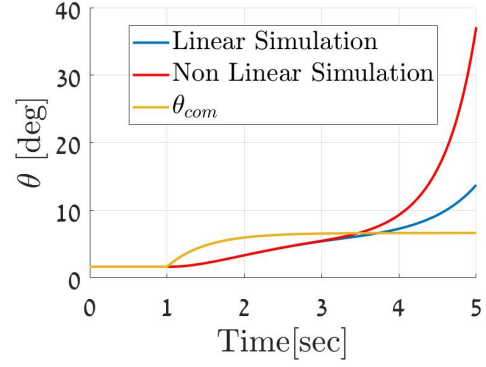
(a)



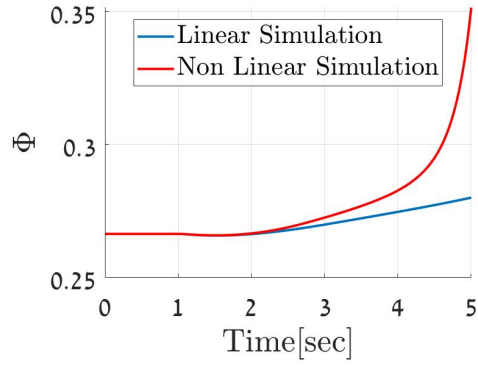
(b)



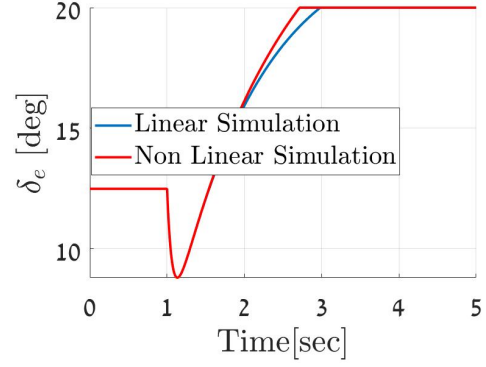
(c)



(d)



(e)



(f)

Figure 13: Response of States and Inputs to  $5^\circ \theta$  Step Command.

## 7 Conclusions

In this project, a nonlinear model of the longitudinal dynamics of an AHV based on [4] was presented and implemented using MATLAB/SIMULINK. This model was validated by finding a trim condition and then was linearized with respect to it. The resulting linear model was used to devise linear controllers for  $V$  and  $\theta$ . These controllers were tested in several test cases on both the nonlinear and linear models and the results were reviewed.

The results show that our approach of designing relatively simple linear feedback controllers to stabilize and control this highly nonlinear coupled system can work to a certain extent. We were able to stabilize the system and track step signals (with steady-state errors), but the system took a relatively long time to converge and diverged when pushed too far. This shows that linear control methods are limited when dealing with such nonlinear coupled dynamics.

This work lays the foundation for future research on this subject. Future work will focus on the use of nonlinear control methods to achieve better tracking performance. It will implement more realistic models of the AHV, accounting for uncertainties and constraints posed by the coupling of the engine and aerodynamics of the vehicle.

## 8 Appendix

This appendix includes the relevant coefficients for our model and is taken from [4].

**Table A1** Miscellaneous coefficient values

Coefficient	Value	Units
$S$	$1.7000 \times 10^1$	$\text{ft}^2 \cdot \text{ft}^{-1}$
$\rho_0$	$6.7429 \times 10^{-5}$	$\text{slugs} \cdot \text{ft}^{-3}$
$h_0$	$8.5000 \times 10^4$	$\text{ft}$
$h_s$	$2.1358 \times 10^4$	$\text{ft}$

**Table A2** Lift and drag coefficient values

Coefficient	Value	Units
$C_L^\alpha$	$4.6773 \times 10^0$	$\text{rad}^{-1}$
$C_L^{\delta_c}$	$7.6224 \times 10^{-1}$	$\text{rad}^{-1}$
$C_L^0$	$-1.8714 \times 10^{-2}$	—

**Table A3 Drag coefficient values**

Coefficient	Value	Units
$C_D^{\alpha^2}$	$5.8224 \times 10^0$	$\text{rad}^{-2}$
$C_D^\alpha$	$-4.5315 \times 10^{-2}$	$\text{rad}^{-1}$
$C_D^{\delta_z^2}$	$8.1993 \times 10^{-1}$	$\text{rad}^{-2}$
$C_D^{\delta_z}$	$2.7699 \times 10^{-4}$	$\text{rad}^{-1}$
$C_D^0$	$1.0131 \times 10^{-2}$	—

**Table A4 Moment coefficient values**

Coefficient	Value	Units
$z_T$	$8.3600 \times 10^0$	ft
$\bar{c}$	$1.7000 \times 10^1$	ft
$C_{M,\alpha}^{\alpha^2}$	$6.2926 \times 10^0$	$\text{rad}^{-2}$
$C_{M,\alpha}^\alpha$	$2.1335 \times 10^0$	$\text{rad}^{-1}$
$C_{M,\alpha}^0$	$1.8979 \times 10^{-1}$	—
$c_e$	$-1.2897 \times 10^0$	$\text{rad}^{-1}$

**Table A5 Thrust coefficient values**

Coefficient	Value	Units
$\beta_1$	$-3.7693 \times 10^5$	$\text{lb} \cdot \text{ft}^{-1} \cdot \text{rad}^{-3}$
$\beta_2$	$-3.7225 \times 10^4$	$\text{lb} \cdot \text{ft}^{-1} \cdot \text{rad}^{-3}$
$\beta_3$	$2.6814 \times 10^4$	$\text{lb} \cdot \text{ft}^{-1} \cdot \text{rad}^{-2}$
$\beta_4$	$-1.7277 \times 10^4$	$\text{lb} \cdot \text{ft}^{-1} \cdot \text{rad}^{-2}$
$\beta_5$	$3.5542 \times 10^4$	$\text{lb} \cdot \text{ft}^{-1} \cdot \text{rad}^{-1}$
$\beta_6$	$-2.4216 \times 10^3$	$\text{lb} \cdot \text{ft}^{-1} \cdot \text{rad}^{-1}$
$\beta_7$	$6.3785 \times 10^3$	$\text{lb} \cdot \text{ft}^{-1}$
$\beta_8$	$-1.0090 \times 10^2$	$\text{lb} \cdot \text{ft}^{-1}$

## References

- [1] Bilardo, V. J., Curran, F. M., Hunt, J. L., Lovell, N. T., Maggio, G., Wilhite, A. W., and McKinney, L. E. “The benefits of hypersonic airbreathing launch systems for access to space”. In: *39th AIAA/ASME/SAE/ASEE Joint Propulsion Conference and Exhibit* (2003). DOI: [10.2514/6.2003-5265](https://doi.org/10.2514/6.2003-5265). URL: <https://arc.aiaa.org/doi/10.2514/6.2003-5265>.
- [2] Marrison, C. I. and Stengel, R. F. “Design of robust control systems for a hypersonic aircraft”. In: *Journal of Guidance, Control, and Dynamics* 21.1 (1998), pp. 58–63. ISSN: 15333884. DOI: [10.2514/2.4197](https://doi.org/10.2514/2.4197). URL: <https://arc.aiaa.org/doi/abs/10.2514/2.4197>.
- [3] Xu, H., Mirmirani, M. D., and Ioannou, P. A. “Adaptive sliding mode control design for a hypersonic flight vehicle”. In: *Journal of Guidance, Control, and Dynamics* 27.5 (2004), pp. 829–838. ISSN: 15333884. DOI: [10.2514/1.12596](https://doi.org/10.2514/1.12596).
- [4] Parker, J. T., Serrani, A., Yurkovich, S., Bolender, M. A., and Doman, D. B. “Control-Oriented Modeling of an Air-Breathing Hypersonic Vehicle”. In: *AIAA Journal of Guidance, Control and Dynamics* 30.3 (2007), pp. 856–869. ISSN: 15333884. DOI: [10.2514/1.27830](https://doi.org/10.2514/1.27830). URL: <https://arc.aiaa.org/doi/abs/10.2514/1.27830>.
- [5] Khalil, H. K. *Nonlinear Control*. Vol. 406. Pearson New York, 2015.
- [6] Fiorentini, L., Serrani, A., Bolender, M. A., and Doman, D. B. “Nonlinear Robust Adaptive Control of Flexible Air-Breathing Hypersonic Vehicles”. In: *AIAA Journal of Guidance, Control and Dynamics* 32.2 (2009), pp. 401–416. ISSN: 15333884. DOI: [10.2514/1.39210](https://doi.org/10.2514/1.39210). URL: <https://arc.aiaa.org/doi/abs/10.2514/1.39210>.
- [7] Fiorentini, L. and Serrani, A. “Adaptive restricted trajectory tracking for a non-minimum phase hypersonic vehicle model”. In: *Automatica* 48.7 (2012), pp. 1248–1261. ISSN: 00051098. DOI: [10.1016/J.AUTOMATICA.2012.04.006](https://doi.org/10.1016/J.AUTOMATICA.2012.04.006).